

Particle Image Velocimetry

Pascal Aeschi, Sebastian Lang, Xeno Meienberg

Experimental Methods for Engineers
 ETH Zürich, D-MAVT, Group 14 - 22.11.2018

Abstract

With the growing evolution of numerical methods and imaging processes in the last century up to this day, particle image velocimetry emerged as one of the most convenient optical techniques in order to study instantaneous flow fields. Without any extensive calibration of the experimental setup, one should be able to find good approximations to the velocity field. In a series of images, we studied the Marangoni Effect in paraffin oil. We recorded the positions of multiple particles in a light sheet at different times and processed accordingly the most probable shifts these particles make from one instance to another. The average of possible velocities respectively most probable displacements would most likely represent the resulting vector field. By adjusting our parameters and filters in terms of window, subwindow and correlation map sizes, allowable maximal shifts and threshold for correlation peaks, our analysis inherently yielded pretty accurate approximations.

1. Experimental Setup and Conditions

The core elements of PIV measurements are separated into two main groups: the experimental components and the recording setup. In this case we are trying to describe and visualize the so called Marangoni Effect. Two distinct phenomena take place when temperature differences are present in a fluid. More commonly known is buoyancy, which causes lower density areas to move opposite to the direction of the gravity field and vice-versa higher density areas. The Marangoni effect is weaker and driven by the temperature dependance of surface tension. Similarly, a flow is established from regions of low surface tension to regions of high surface tension, which means from hot areas to cold areas of the fluid. We generate this type of flow in our flow cell as seen in Fig. 1.

The Flow Cell

By heating light mineral oil on one side of a rectangular glass cell with negligible depth and attaching a copper heat sink on the other side of the cell, we generate a flow. In order to trace the flow, it is important to use particles with similar flow properties as the working fluid in addition to being able to scatter the incoming light. In this case we use polymer spheres. We assume a zero heat flux boundary condition on the top and bottom faces of the cell, due to relatively poor heat conduction in contrast to the right and left sides.

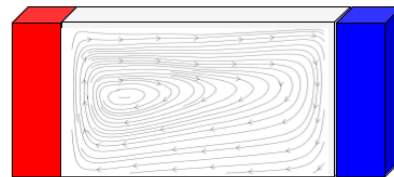


Figure 1: Illustration of the Marangoni Effect in a cell containing paraffin oil and tracers made of polymer

We assume a zero heat flux boundary condition on the top and bottom faces of the cell, due to relatively poor heat conduction in contrast to the right and left sides.

Illumination

In order to conduct the measurement in one plane, i.e. a two dimensional flow, we illuminate the flow volume by creating a light sheet. A diode laser with a wavelength of 670nm produces a beam which goes through a so called Powell lens, which is able to create a uniform light distribution across the sheet. According to studies, it prevents blurry imaged particles just above or below the focussed plane. Therefore, the pollution of our PIV images can be suppressed [Stamhuis (2006)]. Since we only deal with particle displacements of small moduli, we can freeze the instantaneous flow field via the camera shutter. If we studied phenomena at much higher velocities e.g. in wind tunnels, the shutter capability would not suffice, thus high pulsed lasers would help to isolate acceptable images.

Camera

The device we use to record PIV data with is a digital camera. It must fulfill a few key properties to qualify for PIV experiments. First of all it needs a global shutter, meaning it should expose all pixels simultaneously instead of row by row as seen in rolling shutters in order to avoid any distortions. Secondly the sensor needs to have a specific architecture which enables it to have short dead times in between frames by giving each pixel the ability to expose a second frame while the first is still being read out from its own storage area. Finally, it needs to have sufficient resolution which is not a big issue anymore nowadays.

Synchronization

As the camera has a technical limit to how short the exposure time can be, we can artificially make it shorter by only illuminating the test cell during a fraction of the exposure time through timing the pulses of the laser, as depicted in Fig. 2. To achieve this, we use a multi channel pulse timer which is connected to both the camera and the laser.

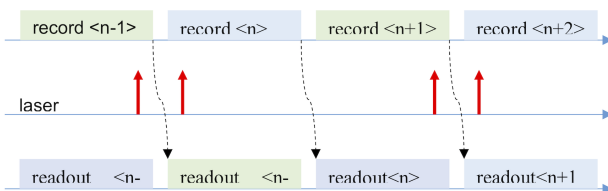


Figure 2: Chronological sequence of operations for the appropriate recordings [Roesgen (2018)]

Computation of the velocities

Following steps are made - qualitatively - in order to determine the velocities of our obtained data

1. Convert our pictures from the light sheet into a matrix, for which every pixel inhibits an intensity value
2. Subtract the minimal intensities in order to shift the minimal intensities to zero such that the relative differences are always referred to the minimum, which is the background
3. Define a meshgrid of sections of our pixels with a defined width and height from a vector containing the interrogation window size. These windows represent one point in a defined meshgrid, quasi a binning of an area of pixels
4. In each of the interrogation windows, smaller sub-windows (inhibiting smaller groups of particles) are

generated. The reason for the search of groups rather than singular particles is that it would be hard to find the identical particle in a densely seeded flow.

5. When we compare two images, we try to compare within each interrogation window their respective subwindows. Here, the correlation takes place. This generates a correlation map for every subwindow and therefore the highest probability of a possible shift. This is done in both dimensions - horizontally and vertically
6. In order to make the process more accurate, we can do a so called “sub-pixel interpolation”. This is done since particles i.e. the resulting peaks in the correlation map are most of the time larger than one pixel and would occupy multiple pixels at once. By fitting a suitable function, for example a two dimensional gaussian near of the correlation maximum, higher accuracy is achieved [Stamhuis (2006)]
7. The computed shifts in both horizontal and vertical direction represent the velocity vector given the time between both shifts is known as well

This procedure is always made for two images. A more accurate picture can be achieved if we do the comparisons for sufficiently enough data sets. Averaging the corresponding data would therefore be an intuitive approach. In this lab exercise, two approaches were identified and executed.

Direct vector map averaging

This ansatz is made by averaging the displacements at each grid point. We did this by stacking all vectors onto each other which resulted into a three-dimensional array containing all vector maps. The maps were averaged by the mean over all points stacked onto each other as seen the provided Matlab script.

Correlation Averaging

The overall principle was, instead of averaging all vectors, the correlation functions would rather be added up if we feed in the weighted correlation average of the previous data. The predefined Matlab routine *PIV_base* would then search for maximum value of the added peaks and then use the distance to the peak as the absolute displacement. For this procedure, we implemented a moving average routine. The average of the correlation map calculated by multiplying the respective number of maps associated to each gridpoint, then adding a new map if the threshold is exceeded and then divide by the new number of correlation maps.

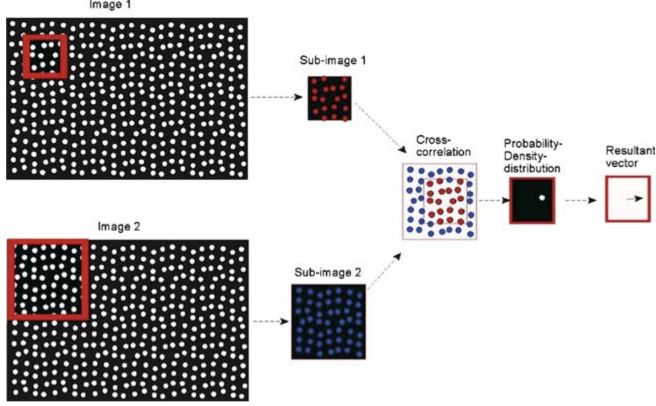


Figure 3: Cross Correlation Principle [Stamhuis (2006)] Note: The size of the sub-image can be changed as well, what results into a more reliable probability density function

Correlation - Mathematical Background

As explained above, the pattern matching of two sub-windows is made by using a similarity criterion. The Fast Fourier Transform (FFT) is used to correlate subwindows with each other. This algorithm is commonly used to transform the interrogation window and subwindow into the complex domain. There, the product - the convolution, to be more exact - of the two windows is generated and transformed back into the real domain. Literature suggests that one should always use subwindow sizes of powers of two. This comes from the fact that fast fourier transforms can be computed in a more efficient way [Cooley and Tukey (1965)].

One can imagine the correlation procedure as a shift of a smaller subwindow of the latter image over the interrogation window of the first one and computing how good both images match at every point within the interrogation window. This procedure is briefly illustrated in Fig. 3.

Mathematically, the correlation coefficients are calculated as follows

$$\rho_{kl} = \frac{\text{Cov}(p_{i,j}, q_{i+k,j+l})}{\sqrt{\text{Var}(p_{i,j}) \text{Var}(q_{i+k,j+l})}} \quad (1)$$

$$\text{Cov}(a_{i,j}, b_{i,j}) = \frac{1}{MN-1} \sum_{m=0}^M \sum_{n=0}^N (a_{i+m,j+n} - \langle a \rangle_{i,j})(b_{i+m,j+n} - \langle b \rangle_{i,j}) \quad (2)$$

$$\text{Var}(a_{i,j}) = \text{Cov}(a_{i,j}, a_{i,j}) \quad (3)$$

$$\langle a \rangle_{i,j} = \frac{1}{MN} \sum_{m=0}^M \sum_{n=0}^N a_{i+m,j+n} \quad (4)$$

Our goal is to find correlation coefficients which do reach value 1, which would give us two identical images with their respective shift. In reality, we cannot reach these values, since the groups within the subwindows do

not perfectly flow together as a group. The correlation map of the comparison of two images evidently does only give a probabilistic, rather than an exact vector field. For a larger set of images, the error for an arbitrarily chosen image pair for the computations should decrease by averaging over the whole data set.

Interframe Separation Time

If we want to estimate the appropriate separation time between two images, we can use a simple dimensional analysis, for which we can calculate implicitly the looked for time. It follows

$$\Delta t = \frac{L}{N_{pix} u_{max}} \delta_{max} \quad (5)$$

Since the given characteristic length ratios are given, the only parameters left that we can really adjust are the maximal values of velocities and displacements. Given from the handout a chosen upper bound for displacement of 10 px would give a very accurate result including sub-pixel interpolation. We assumed that the flow velocity would reach its maximum of about 0.5 mm/s , which resulted into a separation time of 0.7789 s . Therefore, as an approximation we chose 0.8 s which equals the time between four successive images. For later analysis, we calibrate the separation time continuously to study the effects of the parameter in the computations.

2. Results and Discussion

Window Parameters and Grid Sizes

For the computation of our two-dimensional flow, we chose the parameters for the post processing step as listed in Tab.1. The reasoning for the interrogation size was as explained, that the FFT does work much more efficiently on window sizes of 2^N [Cooley and Tukey (1965)]. In addition, a higher density of particles in an interrogation frame should lower the probability of errors [Kiger (2015)]. As well, the correlation peaks are proportional to the particle density [Westerweel (1997)]. We chose an interrogation window of 64×64 , since the resulting grid is 39×73 . For the image frame dimensions of about $45 \times 24 mm$, every grid point will therefore cover at least every mm . A choice of an interrogation window of 32×32 would have yielded a higher resolution, but the computational effort would have increased as well. This is one of the tradeoffs which determined the choice of our given window size. The maximum window shift was chosen so that high accuracy was achieved. It is said that an a priori window shift between two images is implemented

in order to detect displacement values larger than the limit of the maximum shifts [Roesgen (2018)]. In addition, this would generate an oversampling step which also contributes to better results [Stamhuis (2006)]. The subwindow shifts between correlation evaluations was defined to be 16×16 . This follows from given design rules [Roesgen (2018) and Kiger (2015)]. As our sub-pixel Interpolation method, we chose a Gaussian fit, since it has been proven very reliable as a method to eliminate peak locking [Westervel (1997)], which we prove experimentally later on. The thresholds for acceptable correlation maps were determined by trial and error and was mostly the main calibration parameter in order to find acceptable velocity, ergo correlation, curl angular and divergence contour plots.

Table 1: Chosen Parameters for the Post Processing in MATLAB

Interrogation Window Size - wxy	64×64
Maximum Window Shift - sxy	10×10
A Priori Window Shift - oxy	2×2
Subwindow Shifts between Correlation Evaluations - gxy	16×16
Threshold: Direct Vector Map Averaging	0.2
Threshold: Correlation Map Averaging	0.3
Resulting Grid Size - xy_grid resp. uv_vecs	39×73
Correlation Map Sizes - 2sxy+1	21×21
Subpixel-Interpolation Mode	Gaussian

Mean Velocities and Streamlines

First of all, the mean velocity map was computed as seen in Fig. 4. From a reference image, the *pixel to mm* ratio was computed. Additionally, the shifts had to be divided by the separation time in order to match the scales of the true velocities. One can see that the highest velocities tend to be near the Kapton heater. The velocities diminish in the middle of the test cell and towards the boundaries at the top and bottom, this indicates a laminar viscous flow. Later on, the streamlines will give more information about the general trajectory of the particles within the flow.

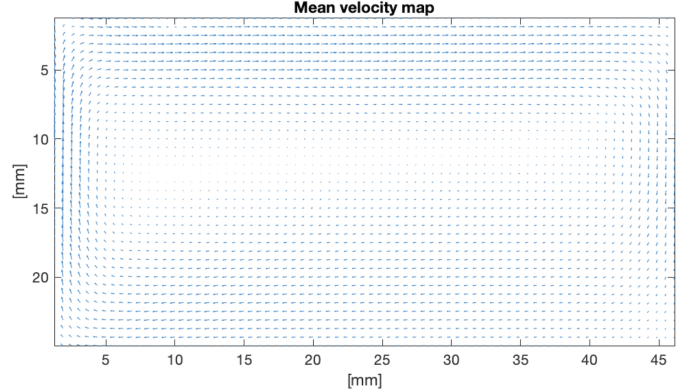


Figure 4: Computed velocity vectors for the test cell: Since the resulting maps for both averaging methods are indistinguishable optically, one can assume similar behavior for each case

The resulting streamlines for the given parameters are shown in Fig. 4 and 5. One can see a more or less non-disturbed flow, which curl around a certain area close to the Kapton heater. The Marangoni effect is therefore intact, the particles travel nearly parallel to each other between both walls. While comparing the figures, one can see that the computation of the average of all vector maps yields nearly as many streamlines as for the correlation average method on the global outer flow, yet towards the center of the rotation, at least one additional streamline is resolved.

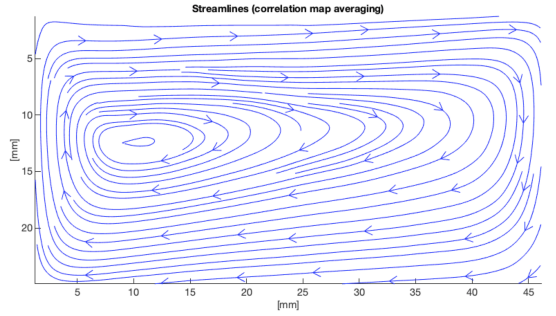


Figure 5: Resulting streamlines in the test cell for the correlation map averaging technique

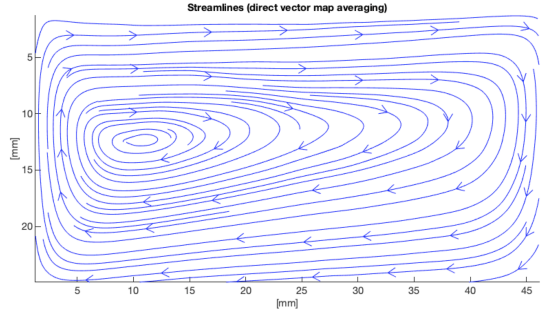


Figure 6: Resulting streamlines in the test cell for the direct vector map averaging technique

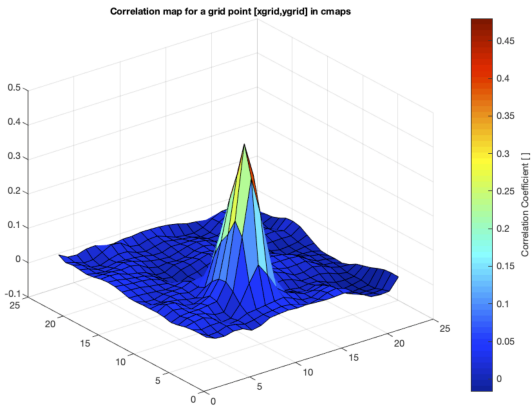


Figure 7: Example of a correlation map, where the peak indicates the highest probability shift

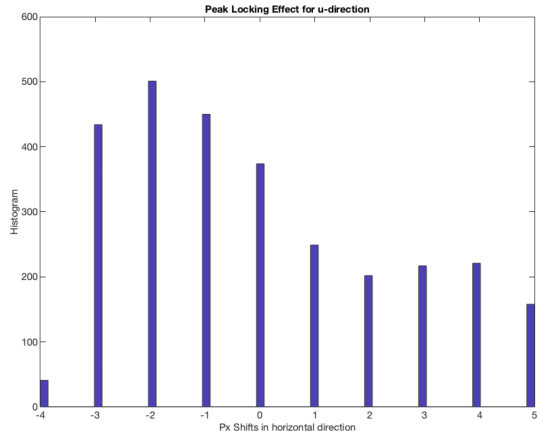


Figure 8: Illustration of the “peak locking effect”. The disabling of sub-pixel interpolation causes a bias of the displacement towards integer values

The averaging of the correlation maps yielded maps of small probability, since the sum of multiple correlation maps also added surrounding noise. Therefore, a correlation coefficient filter of 0.3 was determined as one of the best parameters in order to compute the complete vector field without any missing or outlier vectors. An example of how one of these correlation maps is given in Fig. 7

When we computed the velocities at higher correlation thresholds, we obtained either singularities in the case of the mean of all vectors or strong drifting vectors in the case of the correlation map average method. These distortions changed the calculations of the resulting streamlines and second order quantities drastically. Evidently these calculations did not match our observations during the experiment.

As well, while studying the effects of sub-pixel interpolation, our goal was to determine what the effects were if we used a Gaussian interpolation. The effect of sub-pixel interpolation is portrayed in figures 8 and 9 for all horizontal pixel shifts. The so called “peak locking effect” as introduced in the beginning comes to effect here. This also makes sense if considered that the size of our particles, which were given to have an approximate diameter of $50 \mu m$. From the length-pixel ratio one can show that the diameter would have dimensions around $1.28 px$. It follows that if a particle is partly on one of two or multiple pixels in one frame, the calculations (FFT, convolution, inverse FFT) would return integer pixel shifts (Fig. 8). One can see in Fig. 9 that a Gaussian interpolation leads to more accurate pixel shifts.

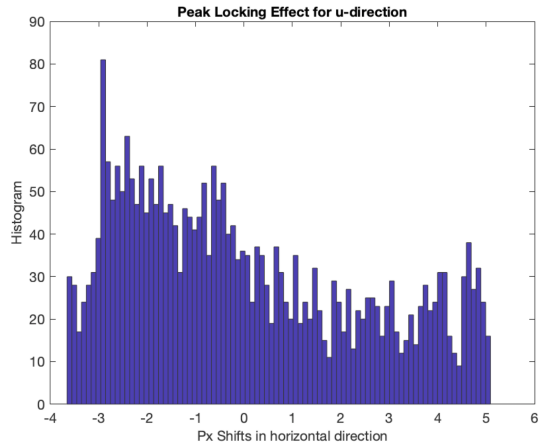


Figure 9: Histogram of the horizontal pixel displacements for the Correlation Map Averaging Technique. The Gaussian sub-pixel interpolation reduces the peak locking effect

Second Order Quantities

After filtering for acceptable velocities, the second order quantities could now be computed as well. Fig. 10 and 11 display the curl angular velocities, colored in the spectrum of values varying between around -0.08 and $0.08 \frac{1}{s}$. Slight differences between both averaging methods can be seen if one observes the the center as well as at the surface of the cell. The rotation of a single particle is especially increased at the hot edge and minimized as soon as the migration towards the opposite cold edge begins. In fact, particles on the surface rotate in the negative direction. The divergence contour plots of both methods show very similar results, which qualitatively do not differ at all, we only refer to one plot (Fig 12). Here, the areas of different color show the level of how strong a particle located at a given point would diverge away from the given point.

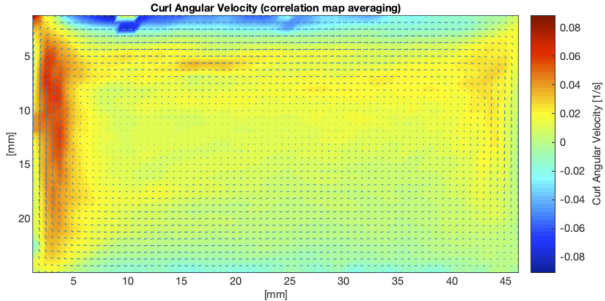


Figure 10: Curl angular velocity map and velocity field. The coloring illustrates the angular velocities which act on the particles in the Marangoni cell

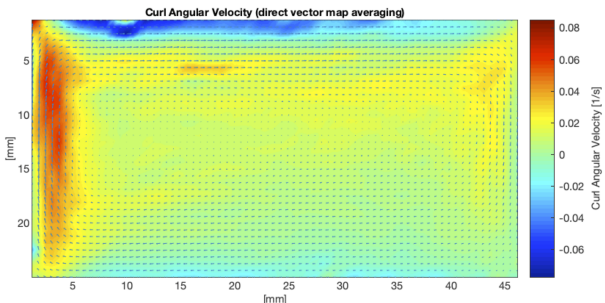


Figure 11: Corresponding Curl Angular Velocity Map and Velocity Field for the Direct Vector Map Averaging Method

Furthermore, it is known from theory that from the material derivative, it follows for incompressible flows that the divergence must be zero. We can see that this is clearly not the case for the entire section. In fact, fluctuations are visible. At the upper surface, two diametral divergence contours are visible.

3. Conclusions and Outlook

With two different methods, we approximated the velocities for our flow cell in a very acceptable range. For our calculations, different threshold values for acceptable correlations were used. It could be seen that for larger cor-

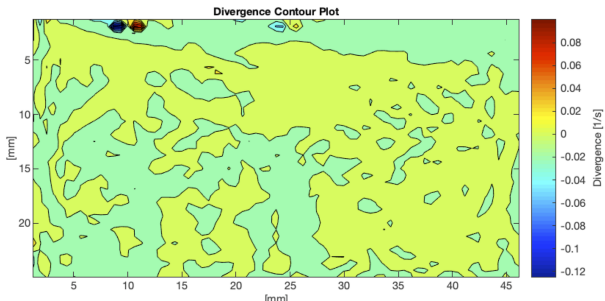


Figure 12: Divergence contour plot for the correlation map averaging method

relation thresholds, the calculations yield either distorted or zero velocities. This phenomenon might come from the fact, that we deal with quite a lot of noise and therefore the overall probability is very smoothly spread throughout the possible displacement map. On the other hand, the acceptance of too high correlation values does also include a risk. High probabilities could lead to computations which do not coincide with the general flow, outliers with high probabilities would shift the average into the wrong direction. The argument of averaging just over all maps in both methods would also introduce problems, coming from the fact that the distinction from noise and the true shift would be very small. This is one key tradeoff one has to consider. Therefore, the use of the correlation threshold as a filter is a factor which always has to be carefully dealt with.

The peak locking effect could be shown figuratively and that a sub-pixel interpolation scheme is always important as soon as the particles do have larger diameters than the pixel size of given imaging devices.

The implementation of other algorithms, such as residual analysis by interpolating wrongfully computed or rejected velocities would have improved our results further.

Even though a FFT was used to calculate all crosscorrelations, the overall runtime for our problem on a standard computer was quite long given the fact that we studied two-dimensional flows in a stationary, very slow flow. A faster computer would have given us more time or a higher resolution if needed. For far more complex studies, a very fast computing device or a more efficient algorithm could optimize this velocimetry technique.

A disadvantage of our PIV setup is that one can only study two-dimensional flows. On top of that, we also did not account for the fact that the tracers would also be able to travel in and out of the plane generated by the laser sheet. A solution of this problem would be an additional camera setup and measuring the trajectories from different angles, a measurement method known as “Stereo PIV”. The introduction of tracer particles into the system, even if they would cause negligible distortions, might also be problematic. For different fluids, it may be more or less difficult to find particles which do not match with the density of the studied fluid.

In conclusion, Particle Image Velocimetry has many advantages over other velocimetry techniques, such as its predecessors, e.g. Laser Doppler or Ultrasonic Doppler methods. With the improvements in imaging and computing devices from recent decades, automatization of this process is possible and less calibration is necessary in order to gain knowledge of various flows.

4. References

Cooley, J. W., Tukey, J. W., 1965. An algorithm for the machine calculation of complex Fourier series. *Math. Comp.* 19, 297–301.

URL <https://doi.org/10.2307/2003354>

Kiger, K., 2015. PIV Basics: Correlation. Online.

URL <http://www.civil.ist.utl.pt>

Roesgen, T., October 2018. Particle Image Velocimetry, Version 2.1.

ETH Zürich.

Stamhuis, E. J., Dec 2006. Basics and principles of particle image velocimetry (piv) for mapping biogenic and biologically relevant flows. *Aquatic Ecology* 40 (4), 463–479.

URL <https://doi.org/10.1007/s10452-005-6567-z>

Westerweel, J., 1997. Fundamentals of digital particle image velocimetry. *Measurement Science and Technology* 8 (12), 1379.

URL <http://stacks.iop.org/0957-0233/8/i=12/a=002>